A SunCam online continuing education course

Filters and Equalizers©

By

Raymond L. Barrett, Jr., PhD, PE
CEO, American Research and Development, LLC

1.0 Filters and Equalizers Introduction

This course will define the notation for roots of polynomial expressions describing Linear-Time Invariant (LTI) systems in the frequency domain, and relate the operator notation to the time-domain response using complex exponential notation. A single pole circuit will be introduced and responses analyzed in the frequency domain and time domain. An ideal delay will be introduced for comparison and to set a reference for step response behaviors.

Polynomial root locations will be described in the complex ***s***-plane and complex conjugate pairs plotted and described using (ω_0, ζ) notation as well as (τ_0, Q) notation. Phasor notation will be introduced for evaluation of steady-state sinusoidal excitation of transfer functions. Second-order, complex conjugate pole pairs are introduced and the asymptotic behaviors developed and contrasted to the single-pole behaviors in magnitude, phase, and group delay attributes. Straight-line approximations are produced and the errors of approximation discussed.

Classical Butterworth, Chebyshev, and Bessel filters are introduced and the construction formulae developed. The Cauer filter is also illustrated, but mathematical development not included. Frequency domain and time domain responses are developed using a 4^{th} design form as representative of even-order forms and a 5^{th} order design as representative of odd-order forms. Only the 5^{th} order Bessel filter example will be synthesized from the equations. A 5^{th} order equalizer will be developed for the 5^{th} order Chebyshev and Cauer filter and shown to provide equivalent results. An additional pole pair will be added to the 5^{th} order equalizer and the justification and improvements noted. Transformations will be discussed to convert low-pass prototype designs to high-pass and band-pass filters.

The course is designed for a practicing engineer seeking a capability for designing and specifying filters and equalizers for frequency domain and time domain applications.

2.0 Notation

Following in the path of intellectual giants, we adopt the Laplace exponential and Fourier complex notations for describing the signals and the systems we employ. Using the notations, we can accurately represent signals in the time domain, as well as transform to the frequency domain for spectral analysis. We define a signal's impulse response as:

$$V_x(t) = A_x e^{st} \qquad [2.0]$$

Allowing the coefficient ***s*** to be a complex number permits the describing equation [2.0] to be representative of growing or declining exponential waveforms employing the real component, as well as periodic sinusoidal waveforms employing the imaginary component, both in the time and frequency domains.

We employ the impulse response as a time-domain descriptor, but evaluate instead the integral of the impulse response or step response because of the difficulty in forming the infinite-magnitude/unit-area form of the impulse excitation. The unit step is more intuitive and easier to formulate for time-domain simulation.

We describe Linear, Time-Invariant (LTI) systems using a rational polynomial descriptive equation of the form given in equation [2.1] below.

$$\frac{V_{out}(s)}{V_{in}(s)} = H(s) = \frac{N(s)}{D(s)} \qquad [2.1]$$

We adopt the classical approach to system description with the roots of ***N(s)*** = 0 defined as zeroes because the transfer function is zero at those root locations, and the roots of ***D(s)*** = 0 defined as poles because the limit of the transfer function is infinite at those root locations and possibly because the magnitude resembles an infinite-height tent-pole under the "fabric" of the ***s*** domain magnitude surface around that location. The degree of N(s) is less than or equal to the degree of D(s) for a realizable system, and each can be factored into first or second order factors.

$$(s + \sigma) \qquad [2.2]$$

A first-order factor in "***s***" transforms to the time domain with the exponential impulse response expressed in equation [2.0] above. The second order factor in "***s***" expressed in equation [2.3] below has three possible cases, depending on the solution of its quadratic equation.

$$(s^2 + bs + c) \qquad [2.3]$$

$$s = -\frac{b}{2} \pm \frac{\sqrt{b^2 - 4c}}{2} \qquad [2.4]$$

In equation [2.4], the square root contains a term known as the discriminant. There are three cases for the value of that discriminant, including positive, zero, or negative values. If the discriminant is positive, the second-order term can be factored into two distinct first-order factors with unequal real roots. If the discriminant is zero, the second-order term can be

factored into two equal first-order factors with two identical repeated roots. If, however, the discriminant is negative, the solution requires a square root of a negative number with an imaginary solution; hence two complementary conjugate root locations. If $4c > b^2$, we have:

$$s = -\frac{b}{2} \pm j\frac{\sqrt{4c - b^2}}{2} \qquad [2.5]$$

To cover all cases, we define every root to be of the form given in equation [2.6] below, with either the real σ_{root} or ω_{root}, possibly zero.

$$s_{root} = \sigma_{root} + j\varpi_{root} \qquad [2.6]$$

Root locations contain information about the transfer function behavior in both time and frequency domains. To characterize the response of a system, we employ the "step" response of the system in the time domain and the magnitude-phase response of the Bode plot in the frequency domain. To illustrate, we utilize first a single pole resistor-capacitor (RC) system shown in figure 2.0 below, and contrast its behavior with an ideal delay.

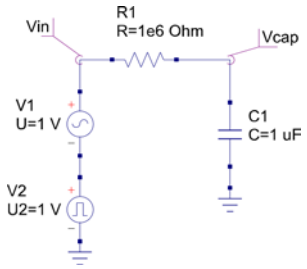

2.0 The Single-Pole RC Circuit Schematic

For the circuit shown in figure 2.0 above, we analyze the response as a "voltage-divider" using the ratio of impedances as follows:

$$Z_R = R = 1 \bullet 10^6 \Omega \qquad [2.7]$$

$$Z_C = \frac{1}{Cs} = \frac{1}{1 \bullet 10^{-6} s}\Omega \qquad [2.8]$$

$$\frac{V_{cap}}{V_{in}}(s) = H(s) = \frac{Z_C}{Z_C + Z_R} = \frac{\frac{1}{Cs}}{R + \frac{1}{Cs}} = \frac{1}{RCs + 1} = \frac{1}{s + 1} \qquad [2.9]$$

The initial value theorem allows us to calculate:

$$V_{cap}(0+) = Lim\big|_{s\to\infty}\left(s \bullet \frac{1}{s+1}\right) \qquad [2.10]$$

Because the result is indeterminate in the ratio, we apply LHopital's rule, as follows:

$$V_{cap}(0+) = Lim\big|_{s\to\infty}\frac{\partial}{\partial s}\left(\frac{s}{s+1}\right) = Lim\big|_{s\to\infty}\left(\frac{(s+1)-s}{(s+1)^2}\right) = Lim\big|_{s\to\infty}\left(\frac{1}{(s+1)^2}\right) = 0 \qquad [2.10]$$

To evaluate the step response, we use the integral of the impulse response and employ the final value theorem as follows. First, the time domain integral of the impulse response is found as follows:

$$\int_0^t V_x(\lambda)d\lambda = A_x\int_0^t e^{-\lambda/\tau}d\lambda = \int_0^t e^{-\lambda}d\lambda = \left[1-e^t\right] \qquad [2.11]$$

The ***s*** domain integral is found as follows:

$$\frac{1}{s}H(s) = \frac{1}{s(s+1)} \qquad [2.12]$$

The final value theorem allows us to calculate:

$$V_{cap}(t\to\infty) = Lim\big|_{s\to 0}\left(s \bullet \frac{1}{s(s+1)}\right) = Lim\big|_{s\to 0}\left(\frac{1}{(s+1)}\right) = 1 \qquad [2.13]$$

We predict that the final value from both the time-domain and frequency domain will agree and be a value of unity.

We show the time-domain step response behavior in the simulation of figure 2.1 below.

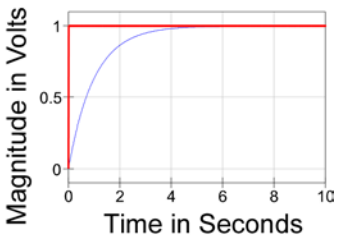

2.1 The Single-Pole RC Circuit Step Response

For the steady-state AC response, we evaluate the transfer function with the $\boldsymbol{s = j\omega}$ substitution as follows:

$$\frac{V_{cap}}{V_{in}}(j\varpi) = H(j\varpi) = \frac{1}{1 + j\varpi} \qquad [2.14]$$

We evaluate the magnitude and phase expressions as follows:

$$\left|H(\varpi)\right| = \frac{1}{\sqrt{1+(\varpi)^2}} \qquad [2.15]$$

$$\Phi_H(\varpi) = -\tan^{-1}(\varpi) \qquad [2.16]$$

We show group-delay as the derivative of the phase expression as follows:

$$\frac{\partial \Phi_H(\varpi)}{\partial \varpi} = -\frac{\partial \tan^{-1}(\varpi)}{\partial \varpi} = -\frac{1}{1+\varpi^2} \qquad [2.17]$$

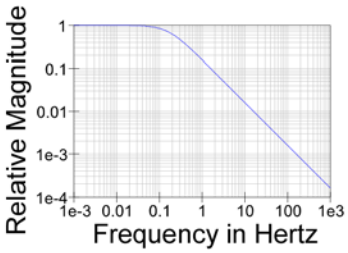

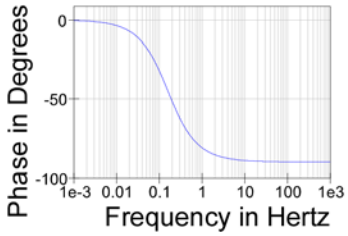

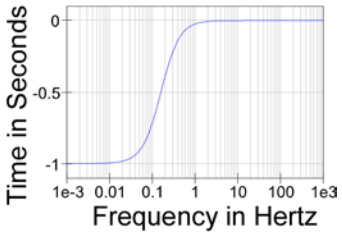

2.2 The Single-Pole RC Circuit Magnitude, Phase, and Group Delay Responses

For contrast, we employ an ideal delay and show its time domain response as follows:

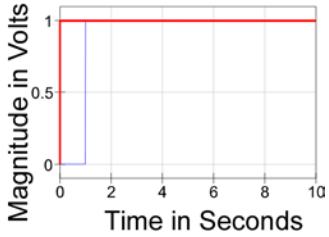

2.3 The Ideal One Second Delay Time-Domain Step Response

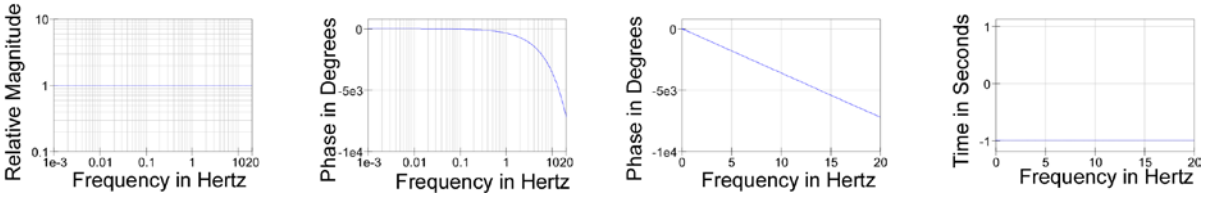

2.4 The Ideal One Second Delay Magnitude, Phase, and Group Delay Responses

From figure 2.4 above, we see that the ideal delay has a uniform magnitude, regardless of the frequency but the single pole shown in figure 2.2 has an asymptotic magnitude of unity only up to its pole frequency associated with the one-second time-constant. The ideal delay has a constant phase expression derivative or group-delay but the single pole has an asymptotic group delay of unity only up to its pole frequency.

The ideal delay is represented as the multiplier e^{-sT} for any positive time index.

3.0 Root Locations

The location of a pole (as well as a zero), in the complex ***s*** plane reveals information about its behavior in both time and frequency domains as we have demonstrated in the section above using a single-pole example.

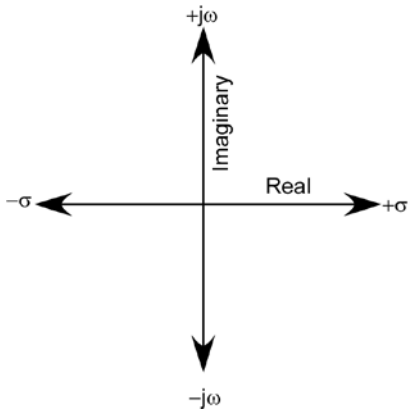

3.0 The Complex S Plane

Real poles are located only on the "Real" axis, but we are mostly interested in poles with a real part that lie in the "Left Half-Plane (LHP)," because they describe the decaying exponentials found in physical systems. Similarly, complex conjugate pole pairs are most often found in the left half plane for practical systems, but some lossless ideal systems may

also include the imaginary axis with a real component of zero. We shall see later that the LHP restriction is not as stringent for the location of zeroes as it is for poles.

We employ two of several conventions for describing the complex-conjugate pairs; following algebraic manipulation to the first canonic form:

$$\left(\tau_0^2 s^2 + \frac{\tau_0}{Q} s + 1\right) \qquad [3.0]$$

$$s_{root} = \frac{-\frac{\tau_0}{Q} \pm \sqrt{\left(\frac{\tau_0}{Q}\right)^2 - 4\tau_0^2}}{2\tau_0^2} \qquad [3.1]$$

$$s_{root} = \frac{-\frac{\tau_0}{Q} \pm \frac{\tau_0}{Q}\sqrt{1-4Q^2}}{2\tau_0^2} \qquad [3.2]$$

$$s_{root} = -\frac{1}{2Q\tau_0}\left[1 \pm \sqrt{1-4Q^2}\right] \qquad [3.3]$$

$$s_{root} = -\frac{1}{2Q\tau_0}\left[1 \pm j\sqrt{4Q^2-1}\right] \qquad [3.4]$$

We have a set of equivalence relations $2\zeta = 1/Q$, and $\tau_0 = 1/\omega_0$ for the alternate canonic form of equation [3.5] as follows:

$$\left(\frac{s^2}{\varpi_0^2} + \frac{2\varsigma}{\varpi_0} s + 1\right) \qquad [3.5]$$

With the alternate form, we have:

$$s_{root} = -\varsigma\varpi_0\left[1 \pm j\frac{1}{\varsigma}\sqrt{1-\varsigma^2}\right] \qquad [3.6]$$

$$s_{root} = -\varsigma\varpi_0 \pm j\varpi_0\sqrt{1-\varsigma^2} \qquad [3.7]$$

We shall see that these two equivalent canonical forms may be used interchangeably, but one or the other may have some advantage for implementation issues.

We show a complex conjugate pole-pair in the s-plane with each canonic representation as follows:

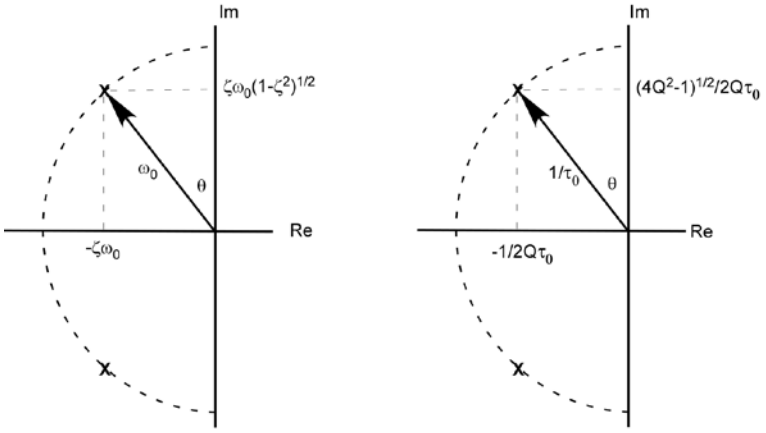

3.1 Complex-Conjugate Pole-Pair in the Complex S Plane (Both Forms Shown)

Note the indicated angle θ in figure 3.0 above is parameterized by the ***tan^{-1}*** relationships as follows:

$$\theta = \tan^{-1}\left(\frac{1}{\sqrt{4Q^2-1}}\right) \qquad [3.8]$$

$$\theta = \tan^{-1}\left(\frac{\varsigma}{\sqrt{1-\varsigma^2}}\right) \qquad [3.9]$$

We will find the θ angle useful in referring to root-pattern loci in filter designs.

We will utilize a "phasor" approach to system behavior for frequency domain evaluation. It leads to a few intuitive tools for the classical system behaviors.

In figure 3.2 below, we illustrate two "phasors" or phase-vectors denoted as $\boldsymbol{p_1}$ and $\boldsymbol{p_2}$ to represent the system response from the two roots shown caused by the excitation from the steady-state excitation locus on the imaginary axis designated as the $\boldsymbol{j\omega}$ point.

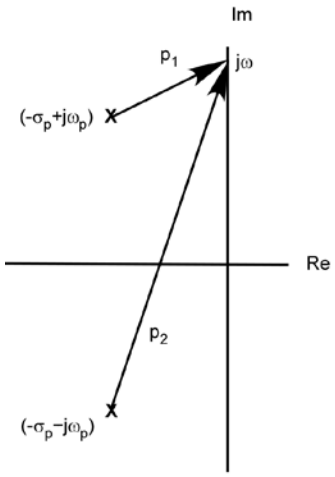

3.2 Phasor Response for a Complex-Conjugate Pair

We represent an evaluation of the partial product shown in equation [3.8] below.

$$X(s) = \left(s + \left(\sigma_p + j\varpi_p\right)\right)\left(s + \left(\sigma_p - j\varpi_p\right)\right) \quad [3.8]$$

The two root locations are:

$$s = -\sigma_p + j\varpi_p \quad [3.9]$$

$$s = -\sigma_p - j\varpi_p \quad [3.10]$$

The two phasors are:

$$p_1 = \sigma_p + j\left(\varpi - \varpi_p\right) \quad [3.11]$$

$$p_2 = \sigma_p + j\left(\varpi + \varpi_p\right) \quad [3.12]$$

We obtain the magnitudes as follows:

$$\left|p_1\right| = \sqrt{\sigma_p^2 + \left(\varpi - \varpi_p\right)^2} \quad [3.13]$$

$$\left|p_2\right| = \sqrt{\sigma_p^2 + \left(\varpi + \varpi_p\right)^2} \quad [3.14]$$

We obtain the phase contributions as follows:

$$\Phi_{p1}(\varpi) = \tan^{-1}\left(\frac{\varpi - \varpi_p}{\sigma_p}\right) \qquad [3.15]$$

$$\Phi_{p2}(\varpi) = \tan^{-1}\left(\frac{\varpi + \varpi_p}{\sigma_p}\right) \qquad [3.16]$$

From this preliminary work, we see that:

$$\left|X(s)\right|_{s\to j\varpi} = \left|p_1\right| \bullet \left|p_2\right| \qquad [3.17]$$

$$\Phi_X(\varpi) = \Phi_{p1}(\varpi) + \Phi_{p2}(\varpi) \qquad [3.18]$$

If we convert the magnitudes to a logarithmic dependency, such as dB, equation [3.17] also becomes a summation. If the phasors describe pole roots, the magnitudes are inverted and result in "negative" or subtractive dB, whereas zeroes result in "positive" or additive dB. Similarly, poles subtract their phase contributions and zeroes add their phase contributions.

4.0 Second-Order Pole Behaviors

The locus of the complex-conjugate pole pairs with constant characteristic frequency and differing damping or "***Q***" presents insights into the placement of loci maps for filters and will be developed in the following sections.

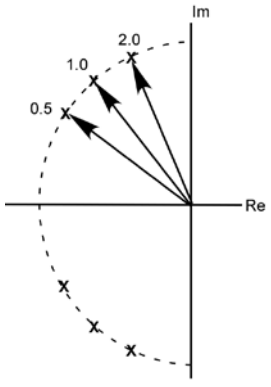

4.0 Complex-Conjugate Pole Pair with Q = 0.5, 1.0, and 2.0 Parameters (Concept)

We have shown in figure 4.0 above a conceptual relationship for the pole locations of a complex-conjugate pole pair with three different "Q" values. The angles are for relative

direction only, but the loci are all on a circle of constant radius. We evaluate the location angles to find the respective values for θ as follows:

$$\theta\big|_{Q=0.5,1.0,2.0} = \tan^{-1}\left(\frac{1}{\sqrt{4Q^2-1}}\right)\Bigg|_{Q=0.5,1.0,2.0} = \tan^{-1}(\infty), \tan^{-1}\left(\frac{1}{\sqrt{3}}\right), \tan^{-1}\left(\frac{1}{\sqrt{15}}\right) \qquad [4.0]$$

$$\theta\big|_{Q=0.5,1.0,2.0} = 90^o, 30^o, 14.5^o \qquad [4.1]$$

In figure 4.0 above, we did not show the precise angles for the "***Q***" values indicated because the ***Q*** = 0.5 value is actually a repeated double-pole exactly on the real axis and difficult to resolve as a pole-pair. In figure 4.1 below, we show the magnitude, phase, and delay characteristics for the same pole-pair collection.

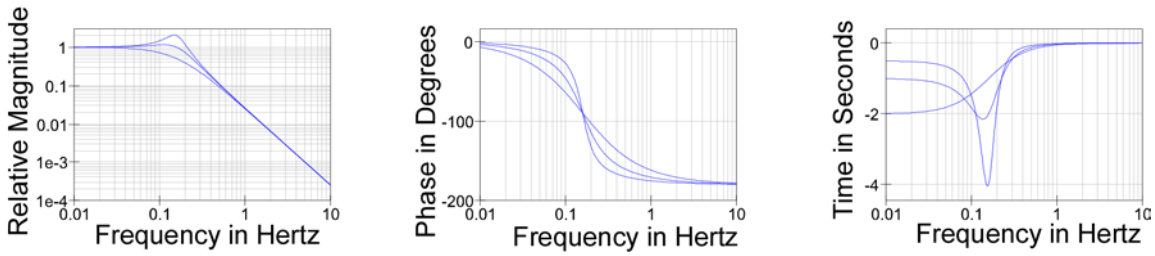

4.1 Pole Pair Magnitude, Phase, and Group Delay with Q = 0.5, 1.0, and 2.0

The transfer function description of the behaviors show in figure 4.1 above is given with equation [3.0] as the denominator of ***N(s)/D(s)*** and its roots as the solution of the D(s) polynomial and N(s) = 1 in the numerator as shown in equation [4.2] below.

$$\frac{N(s)}{D(s)} = \frac{1}{\tau_0^2 s^2 + \frac{\tau_0}{Q} s + 1} \qquad [4.2]$$

For the example, $\tau_0 = 1$, which implies $\omega_0 = 1$, and because $\omega_0 = 2\pi f$, the characteristic frequency ***f*** in Hertz is $1/2\pi = 0.159$ Hertz, as can be identified on the panels of figure 4.1 above. We explore the asymptotic behaviors of figure 4.1 while referring to equation [3.19] to develop those asymptotes. We evaluate equation [4.3] below at frequencies below, at, and above the characteristic frequency in the following using the notation of $\Omega = \omega\tau_0$ as a normalizing parameter.

$$\left|\frac{1}{D(\Omega)}\right|_{s=j\varpi} = \frac{1}{\sqrt{\left(1-\Omega^2\right)^2+\left(\frac{\Omega}{Q}\right)^2}} \qquad [4.3]$$

$$\Phi_{1/D}(\Omega) = -\tan^{-1}\frac{1}{Q}\left(\frac{\Omega}{1-\Omega^2}\right) \qquad [4.4]$$

$$GD(\Omega) = \frac{\partial\Phi_{1/D}(\Omega)}{\partial\varpi} = -\frac{1}{1+\left(\frac{1}{Q}\left(\frac{\Omega}{1-\Omega^2}\right)\right)^2}\frac{\partial\left(\frac{1}{Q}\left(\frac{\Omega}{1-\Omega^2}\right)\right)}{\partial\Omega}\frac{\partial\Omega}{\partial\varpi} \qquad [4.5]$$

$$GD(\Omega) = -\frac{\tau_0}{Q}\frac{1}{1+\left(\frac{1}{Q}\left(\frac{\Omega}{1-\Omega^2}\right)\right)^2}\frac{\left(1+\Omega^2\right)}{\left(1-\Omega^2\right)^2} \qquad [4.6]$$

$$GD(\Omega) = -\frac{\tau_0}{Q}\frac{\left(1+\Omega^2\right)}{\left(1-\Omega^2\right)^2+\left(\frac{\Omega}{Q}\right)^2} \qquad [4.7]$$

We evaluate the asymptotes and characteristic using the limits of Ω = 0, 1, and approaching infinity as follows:

$$\left|\frac{1}{D(\Omega)}\right|_{\Omega\to 0,1,\infty} = +1,+Q,+0 \qquad [4.8]$$

We observe from equation [4.4] above that in the region with values of $\boldsymbol{\Omega} >> 1$, we can reduce equation [4.4] to the approximation in equation [4.9] as follows:

$$\left|\frac{1}{D(\Omega)}\right|_{\Omega>>1} \approx \frac{1}{\sqrt{\Omega^4+\left(\frac{\Omega}{Q}\right)^2}} \approx \frac{1}{\sqrt{\Omega^4}} \approx \frac{1}{\Omega^2} \qquad [4.9]$$

It is this exponential relationship that provides the asymptotic slope of two decades magnitude decrease for every decade of frequency increase and leads us to present figure 4.1

using the logarithmic frequency and magnitude scales. The ratio is the constant slope of negative two decades magnitude per frequency decade. In contrast, the single pole behavior shown in figure 2.2 produced a single decade per decade slope. In our normalized notation, we reproduce the single pole magnitude relationship with equation [4.10] as follows:

$$\left|H(\Omega)\right| = \frac{1}{\sqrt{1+(\Omega)^2}} \qquad [4.10]$$

The asymptote for $\boldsymbol{\Omega} >> 1$ produces the result:

$$\left|H(\Omega)\right|_{\Omega>>1} \approx \frac{1}{\sqrt{\Omega^2}} = \frac{1}{\Omega} \qquad [4.11]$$

We see that equation [4.11] algebraically confirms the single-pole asymptotic behavior previously shown in figure 2.2.

We will use the characteristic of a one-decade magnitude decrease per decade frequency increase per pole to help define frequency selectivity of a collection of poles in a filter.

For the $\boldsymbol{\Phi(\Omega)}$ phase response, we observe in figure 4.1, a relatively symmetrical slope with a nearly arithmetic dependence of phase per decade of frequency variation above and below the characteristic frequency, always with 90º for $\boldsymbol{\Omega} = 1$, independent of the $\boldsymbol{Q}$ value as indicated in equation [4.12] below.

$$\Phi_{1/D}(\Omega)\big|_{\Omega\to 0,1,\infty} = 0,-90^o,-180^o \qquad [4.12]$$

The group delay is determined by the phase slope in equation [4.7], and is evaluated over the range of frequencies in equation [4.13] below.

$$GD(\Omega)\big|_{\Omega\to 0,1,\infty} = -\frac{\tau_0}{Q},-2Q\tau_0,0 \qquad [4.13]$$

We see that the phase slope is proportional to $\boldsymbol{Q}$ at $\boldsymbol{\Omega} = 1$, and the least slope appears for the real poles with the $\boldsymbol{Q}$ = 0.5 value. It is instructive to note that the single-pole behavior exhibits the same shape phase dependency as shown in figure 2.2 above, but with the asymptotes given by equation [4.14] below.

$$\Phi_{1-Pole}(\Omega)\big|_{\Omega\to 0,1,\infty} = 0,-45^o,-90^o \qquad [4.14]$$

We observe in both figure 2.2 and figure 4.1 with $\boldsymbol{Q}$ = 0.5, that the arithmetic phase slope can be approximated by a straight-line segment over a two-decade span. We restate equation [4.14] over those restricted limits in equation [4.14] below.

$$\Phi_{1-Pole}(\Omega)\Big|_{\Omega\to\frac{1}{10},1,10} = -5.7^o, -45^o, -84.3^o \qquad [4.15]$$

We are able to use the results of equation [4.15] to infer that a straight-line approximation with the asymptotic value of 0° for frequencies lower than one decade below a pole's characteristic frequency, -90° for frequencies greater than one decade above that pole's characteristic frequency, and -90°/decade slope within the two-decade range is a close approximation of each real-pole's phase characteristic. Further, using the implications we inferred from equation [4.12], we extend the approximation to increase the slope to twice that of a single pole for the complex-conjugate pole pair, but with the slope increased by a multiple of "***Q***" times greater slope magnitude.

We have reproduced the single-pole phase panel from figure 2.2 and the pole-pair phase panel from figure 4.1 into figure 4.2 below and superimposed the approximate straight-line segments in red for comparison.

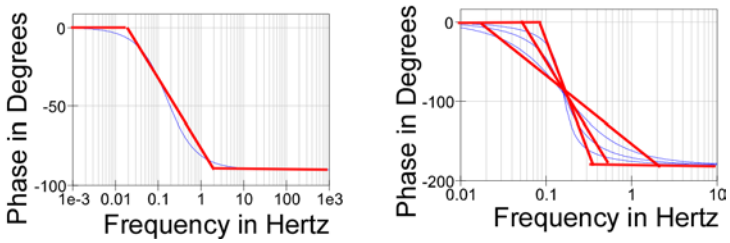

4.2 Single-Pole and Pole Pair Phase with Q = 0.5, 1.0, and 2.0 Approximations

We have already discussed the asymptotic behaviors of the pole magnitude functions and present similar straight-line approximations for the magnitudes in figure 4.3 below. The left panel is the magnitude plot from figure 2.2 and the right panel is the magnitude plot from figure 4.1 and reproduced with the asymptotes from prior discussion.

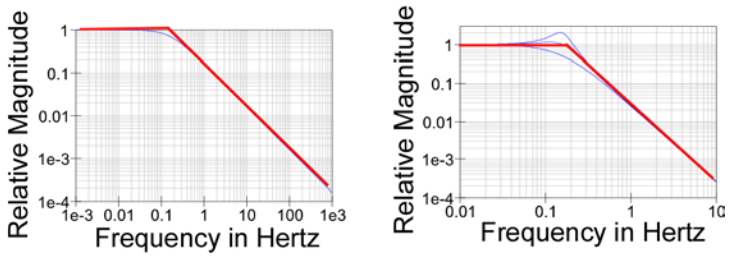

4.3 Single-Pole and Pole Pair Magnitudes with Q = 0.5, 1.0, and 2.0 Approximations

The approximations supported by the results presented in figure 4.1 and figure 4.2, are sufficiently accurate to permit construction of selectivity and phase approximations for complicated filter structures.

In the time domain, we present the results for the complex pole-pair and reproduce the results from the prior figure 2.3 and figure 2.1 shown together in figure 4.4 below.

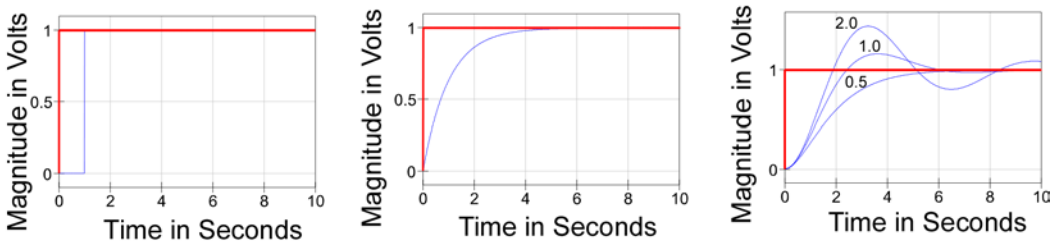

4.4 Delay for Ideal, Single Pole, and Pole Pair with Q = 0.5, 1.0, and 2.0

As shown in figure 4.4 above, the case with two real poles represented with ***Q*** = 0.5 presents twice the delay of the single pole reproduced in the center panel above. The resonant peaking and group delay associated with ***Q*** values of 1.0 and 2.0 presents a resonant overshoot and "ringing" of the step response that become important in dealing with digital signals in band-limited filter structures.

5.0 Some Classical Filter Forms

The classical approach identifies the locus of pole positions according to some desired behavior required for the filter in the time or frequency domain. In this section, we will briefly introduce the Butterworth filter, Chebyshev filter, Inverse Chebyshev filter leading to the Cauer filter, and Bessel filter and show some behaviors in time and frequency domains. We begin with all-pole filters and introduce zeroes. We introduce the maximally flat delay filter and introduce the need for equalizers to obtain good performance in both time and frequency domains.

The N^{th} order Butterworth filter [S. Butterworth, "On the theory of Filter Amplifiers," Wireless Engineer, vol. 7, pp. 536-541, Oct., 1930] has a monotonically decreasing magnitude function as the frequency increases. The characteristic frequency and order, or number of poles parameterizes the lowpass Butterworth filter. A straight-line approximation as discussed in the prior section is usually employed to determine the required number of poles to reject some frequency component at a higher frequency than the characteristic. The ratio of the rejected frequency to the characteristic is calculated and the base-10 logarithm

obtained to determine the number of decades that separate the two frequencies. The required attenuation at the rejected frequency used to determine the requisite attenuation per decades of separation, and thus the minimum number of poles required. For example, we will calculate the order of a Butterworth filter required to provide attenuation by a factor of 1000 at a frequency that is seven times the characteristic frequency. The frequency we must reject is 0.84 decades above the characteristic frequency ($\log_{10}[7] = 0.84$). The rejection factor of 1000 represents three decades ($\log_{10}[1000] = 3$). We need a filter with 3 decades magnitude decrease for 0.84 decades frequency increase, so the minimum ratio is 3/0.84 = 3.57 poles. We do not have the option of fractional poles, so we require a ***4th*** order Butterworth filter.

The Butterworth function is defined as:

$$B_N(\Omega) = \frac{1}{1+\Omega^{2N}} \qquad [5.0]$$

The Butterworth function is used to define the squared-magnitude of a Butterworth filter.

$$\left|H_{B_N}(j\Omega)\right|^2 = B_N(\Omega) = \frac{1}{1+\Omega^{2N}} \qquad [5.1]$$

The definition used in equation [5.1] is obtained indirectly from geometrical constructions in the complex ***s***-plane. We are using the entire ***s***-plane, and express the magnitude function with right-half-plane (RHP), and mirrored left-half-plane (LHP) factors for construction as follows:

$$H_N\left(\frac{s}{\varpi_0}\right)H_N\left(-\frac{s}{\varpi_0}\right)\Bigg|_{s\to j\varpi} = \left|H_{B_N}\left(j\frac{s}{\varpi_0}\right)\right|^2 = \left|H_{B_N}(j\Omega)\right|^2 \qquad [5.2]$$

$$H_N\left(\frac{s}{\varpi_0}\right)H_N\left(-\frac{s}{\varpi_0}\right) = \frac{1}{1+\left(\frac{s}{\varpi_0}\right)^{2N}} \qquad [5.3]$$

The pole locations are defined as the denominator roots:

$$1+\left(\frac{s}{\varpi_0}\right)^{2N} = 0 \qquad [5.4]$$

$$\left(\frac{s}{\varpi_0}\right)^{2N} = -1 = e^{j(2k-1)\pi} \qquad [5.5]$$

The key to Butterworth's derivation is the expression of the higher-order roots of (-1) as an exponential. The exponent of 2N describes the total collection of poles in both the RHP and LHP. We construct the mirror image distribution and use only the stable LHP poles for the filter. The location of poles must consist of a single real pole for ***N*** an odd number, or complex conjugate pole-pairs for ***N*** an even number, due to the nature of poles themselves. The physical realization imposes symmetry on the ***s***-plane locations. The unit magnitude of the exponential in equation [5.5] imposes a locus of a unit circle. We can construct the s-plane map from the information above. We show pole location examples for ***4th*** order and ***5th*** order Butterworth filters in figure 5.0 below.

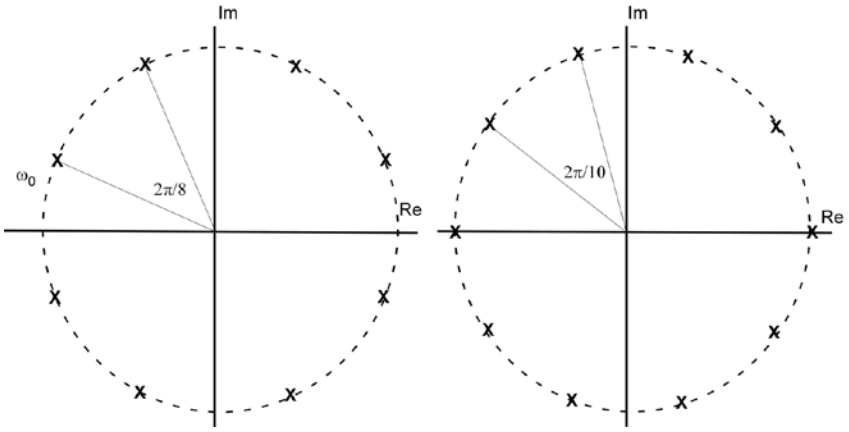

5.0 Butterworth Pole Locations for 4th and 5th Order Filters

From the geometry of the poles on a unit circle, the normalized pole locations are calculated for the LHP locations only. The "***Q***" for each complex conjugate pole pair can be pre-calculated and the radius of the circle is the characteristic ω_0 frequency.

Starting from the pole with the highest ***Q*** factor in each diagram, we see that the incremental angle is always bisected by the imaginary axis. That angle can be deduced to always be π/2N radians. We increment by π/N radians until we reach or exceed π/2 radians and cease calculations without using the last result.

From figure 3.1, we see that a ratio can be used to identify the ***Q*** factor for a complex conjugate pole pair:

$$\tan(\theta) = \frac{1/2Q\tau_0}{\sqrt{(4Q^2-1)}/2Q\tau_0} = \frac{1}{\sqrt{(4Q^2-1)}} \qquad [5.6]$$

$$\left(4Q^2 - 1\right) = \left(\frac{1}{\tan(\theta)}\right)^2 \qquad [5.7]$$

$$Q = \frac{1}{2}\sqrt{\left(\frac{1}{\tan(\theta)}\right)^2 + 1} \qquad [5.8]$$

We calculate the ***Q*** values for the two sets of complex conjugate pole-pairs in table 5.0 below using equation [5.8] above.

Table 5.0 - Butterworth Pole Q factors

4th Order		5th Order	
Angle Radians	**Q**	**Angle Radians**	**Q**
0.392699082	**1.306563**	**0.314159265**	**1.618034**
1.178097245	**0.541196**	**0.942477796**	**0.618034**

We use the same implementation for the Butterworth filters that we employed for the complex conjugate pole-pair characterization but using two instances. We parameterize two sets, one set for the 4th order filter, and the other set for the 5th order filter. We introduce a single pole into the set for the 5th order filter. We then produce the expected results below and obtain the same characteristic frequency as prior examples.

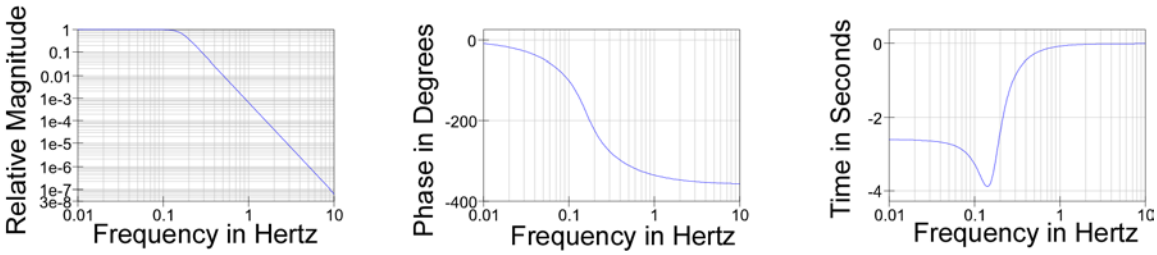

5.1 Magnitude, Phase, and Group Delay for 4th Order Butterworth Filter

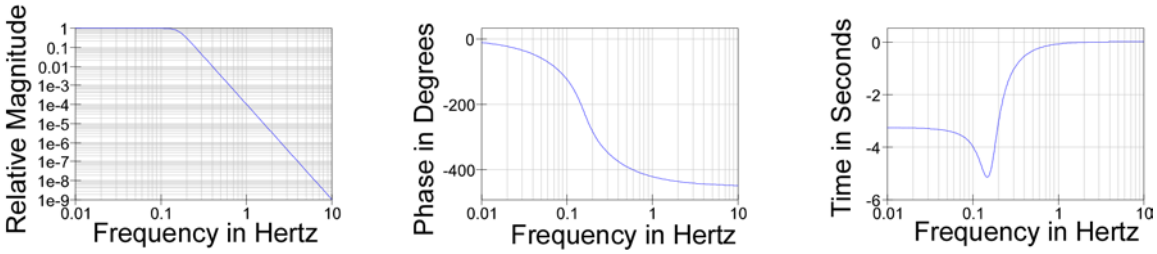

5.2 Magnitude, Phase, and Group Delay for 5th Order Butterworth Filter

In contrast, the 5th order filter achieves a five-decade magnitude decrease per decade of frequency increase where the 4th order filter achieves a four-decade magnitude decrease per decade of frequency increase. That four-decade decrease is sufficient to meet the example requirement of a filter with 3 decades magnitude decrease for 0.84 decades frequency increase. Both the 4th order filter and 5th order filter appear to provide the "maximally-flat" response magnitude of a Butterworth filter.

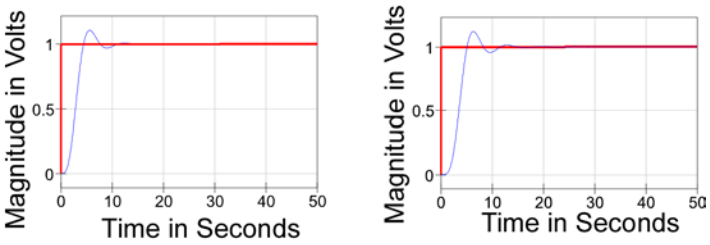

5.3 Step Response for 4th and 5th Order Butterworth Filters

As shown in figure 5.3 above, both the ***4th*** order filter and ***5th*** order filter exhibit the expected resonant peaking and group delay associated with the ***Q*** employed. The resonant overshoot and "ringing" of the step response must be considered in dealing with digital signals in band-limited filter structures.

The Butterworth filter has a monotonically decreasing magnitude function as the frequency increases. It is "maximally flat" in the sense that all derivatives tend to zero as the frequency tends to zero. In contrast, the Chebyshev filter constructs the "passband" from zero to the characteristic frequency with an "equiripple" magnitude by employing Chebyshev polynomials. The ripple, as well as the characteristic frequency and order are parameters of the lowpass Chebyshev filter.

We shall develop a 5th order Chebyshev filter and contrast its behavior with the Butterworth filter above. The Chebyshev polynomial is defined as:

$$T_N(\Omega) = \cos\left(N \cos^{-1}(\Omega)\right) \qquad [5.9]$$

The polynomial is difficult to evaluated directly, but is attacked using a recursive relationship developed from trigonometric identities. First, for ***N*** = 0, and ***N*** = 1, we see:

$$T_0(\Omega) = \cos(0) = 1 \qquad [5.10]$$

$$T_1(\Omega) = \cos\left(\cos^{-1}(\Omega)\right) = \Omega \qquad [5.11]$$

Then, by use of the recursive trigonometric identity:

$$\cos((n+1)x) = 2\cos(nx)\cos(x) - \cos((n-1)x) \qquad [5.12]$$

The higher order polynomials can be defined recursively by:

$$T_{N+1}(\Omega) = 2\Omega T_N(\Omega) - T_{N-1}(\Omega) \qquad [5.13]$$

The polynomials are employed much like the Butterworth case, over the entire s-plane using the magnitude-squared function.

$$\left|H_{T_N}(j\Omega)\right|^2 = \frac{1}{1+\varepsilon^2 T_N^2(\Omega)} \qquad [5.14]$$

The ε parameter provides the ripple scaling value, and depends on the peak-to-peak ripple allowed. For a ripple value A_{Max} expressed in dB (the common measure), we have:

$$\varepsilon = \sqrt{10^{(A_{Max}/10)} - 1} \qquad [5.15]$$

We will develop a ***5th*** order filter with 1dB ripple to contrast with the Butterworth example previously explored. First, we find the ε parameter using equation [5.15] as follows:

$$\varepsilon_{1dB} = \sqrt{10^{(1/10)} - 1} = \sqrt{1.2589 - 1} = \sqrt{0.2589} = 0.5088 \qquad [5.16]$$

We require the ***5th*** order Chebyshev polynomial, so we invoke the recursive definition to extend from the lower orders we have:

$$T_2(\Omega) = 2\Omega T_1(\Omega) - T_0(\Omega) = 2\Omega^2 - 1 \qquad [5.17]$$

$$T_3(\Omega) = 2\Omega T_2(\Omega) - T_1(\Omega) = 2\Omega\left(2\Omega^2 - 1\right) - \Omega = 4\Omega^3 - 3\Omega \qquad [5.18]$$

$$T_4(\Omega) = 2\Omega T_3(\Omega) - T_2(\Omega) = 2\Omega\left(4\Omega^3 - 3\Omega\right) - \left(2\Omega^2 - 1\right) \qquad [5.19]$$

$$T_4(\Omega) = \left(8\Omega^4 - 6\Omega^2\right) - \left(2\Omega^2 - 1\right) = \left(8\Omega^4 - 8\Omega^2 + 1\right) \qquad [5.20]$$

From equation [5.20] and equation [5.14] we have:

$$\left|H_{T_N}(j\Omega)\right|^2 = \frac{1}{1+\varepsilon^2\left(8\Omega^4 - 8\Omega^2 + 1\right)^2} = \frac{1}{1+0.2589\left(8\Omega^4 - 8\Omega^2 + 1\right)^2} \qquad [5.21]$$

Armed with equation [5.21], we can find the poles for this ***5th*** order Chebyshev filter, but we do not have a great insight from a numerical solution. As an alternative, we re-visit the geometry of the ***s***-plane pole locations from a different, but still algebraic direction. We proceed by making a substitution from equation [5.9] that defines the Chebyshev polynomial into equation [5.14] that defines the filter magnitude with the result in equation [5.22] that follows.

$$\left|H_{T_N}(j\Omega)\right|^2 = \frac{1}{1+\varepsilon^2 T_N^2(\Omega)} = \frac{1}{1+\varepsilon^2\left[\cos^2\left(N\cos^{-1}(\Omega)\right)\right]} \qquad [5.22]$$

We know that the Laplace operator "***s***" becomes the Fourier operator "$j\omega$" in the steady-state AC analysis, but we are using the normalized $\Omega = \omega/\omega_0$ substitution. We can make the definition:

$$s \equiv j\,\Omega/\varpi_0 \qquad [5.23]$$

We solve for the relationship:

$$\Omega = \frac{\varpi_0}{j}s \qquad [5.24]$$

We define a complex number ξ as an intermediate variable, but retain the relationship to the roots that define $s = \sigma_p + j\omega_p$ as a location in the ***s***- plane:

$$\xi = \alpha + j\beta \equiv \cos^{-1}\left(\frac{\varpi_0}{j}s\right) = \cos^{-1}(\Omega) \qquad [5.25]$$

Inverting the defined relationship in equation [5.25], we can produce:

$$\frac{\varpi_0}{j}s = \cos(\alpha + j\beta) \qquad [5.26]$$

$$\frac{\varpi_0}{j}\left(\sigma_p + j\varpi_p\right) = \cos(\alpha + j\beta) \qquad [5.27]$$

$$\sigma_p + j\varpi_p = j\frac{1}{\varpi_0}\cos(\alpha + j\beta) \qquad [5.28]$$

Using equation [5.28], we can solve for the pole locations in the ***s***-plane using an identity to provide the needed relationship:

$$\cos(x) = \frac{e^{jx} + e^{-jx}}{2} \qquad [5.29]$$

$$\cos(\alpha + j\beta) = \frac{e^{j(\alpha+j\beta)} + e^{-j(\alpha+j\beta)}}{2} = \frac{e^{-\beta}e^{j\alpha}}{2} + \frac{e^{\beta}e^{-j\alpha}}{2} \qquad [5.30]$$

$$\cos(\alpha + j\beta) = \frac{(\cosh\beta - \sinh\beta)(\cos\alpha + j\sin\alpha)}{2} + \frac{(\cosh\beta + \sinh\beta)(\cos\alpha - j\sin\alpha)}{2} \qquad [5.31]$$

$$\cos(\alpha + j\beta) = \frac{\cos\alpha(\cosh\beta - \sinh\beta) + j\sin\alpha(\cosh\beta - \sinh\beta)}{2} + \frac{\cos\alpha(\cosh\beta + \sinh\beta) - j\sin\alpha(\cosh\beta + \sinh\beta)}{2} \qquad [5.32]$$

$$\cos(\alpha + j\beta) = \frac{\cos\alpha(\cosh\beta - \sinh\beta) + \cos\alpha(\cosh\beta + \sinh\beta)}{2} + \frac{j\sin\alpha(\cosh\beta - \sinh\beta) - j\sin\alpha(\cosh\beta + \sinh\beta)}{2} \qquad [5.33]$$

$$\cos(\alpha + j\beta) = \frac{\cos\alpha\cosh\beta + \cos\alpha\cosh\beta}{2} + \frac{-j\sin\alpha\sinh\beta - j\sin\alpha\sinh\beta}{2} \qquad [5.34]$$

$$\cos(\alpha + j\beta) = \cos\alpha\cosh\beta - j\sin\alpha\sinh\beta \qquad [5.35]$$

We can substitute the relationship derived in equation [5.35] into the prior equation [5.28] to obtain equation [5.36] below.

$$\sigma_p + j\varpi_p = j\frac{1}{\varpi_0}\cos(\alpha + j\beta) = j\frac{1}{\varpi_0}[\cos\alpha\cosh\beta - j\sin\alpha\sinh\beta] \qquad [5.36]$$

$$\sigma_p + j\varpi_p = \frac{\sin\alpha\sinh\beta}{\varpi_0} + j\frac{\cos\alpha\cosh\beta}{\varpi_0} \qquad [5.37]$$

We equate the components as follows:

$$\sigma_p = \frac{\sin\alpha \sinh\beta}{\varpi_0} \qquad [5.38]$$

$$\varpi_p = \frac{\cos\alpha \cosh\beta}{\varpi_0} \qquad [5.39]$$

From equation [5.38] and equation [5.39], we can locate the poles in the ***s***-plane, given the corresponding α and β values.

$$\left|H_{T_N}(j\Omega)\right|^2 = \frac{1}{1+\varepsilon^2\left[\cos^2\left(N\cos^{-1}(\Omega)\right)\right]} = \frac{1}{1+\varepsilon^2\left[\cos^2(N\xi)\right]} \qquad [5.40]$$

From equation [5.40], we identify the poles of the magnitude-squared as:

$$1+\varepsilon^2\left[\cos^2(N\xi)\right] = 0 \qquad [5.41]$$

We factor equation [5.41] as follows:

$$(1+j\varepsilon\cos(N\xi))(1-j\varepsilon\cos(N\xi)) = 1 \pm j\varepsilon\cos(N\xi) = 0 \qquad [5.42]$$

We solve equation [5.42] as follows:

$$\cos(N\xi) = \pm\frac{1}{j\varepsilon} = \cos N(\alpha + j\beta) \qquad [5.43]$$

We again employ equation [5.35] as follows:

$$\cos(N\xi) = \cos N\alpha \cosh N\beta - j\sin N\alpha \sinh N\beta = \pm\frac{1}{j\varepsilon} \qquad [5.44]$$

We equate real and imaginary parts as follows:

$$\cos N\alpha \cosh N\beta = 0 \qquad [5.45]$$

$$\sin N\alpha \sinh N\beta = \pm\frac{1}{\varepsilon} \qquad [5.46]$$

We solve equation [5.45] by noting that ***cos(x) = 0*** for ***x = +/-π/2*** and points with increments of π added. We simplify as follows:

$$\cos N\alpha\Big|_{N\alpha=\pm\left(\frac{\pi}{2}+k\pi\right)}=0 \qquad [5.47]$$

$$N\alpha=\pm(2k-1)\frac{\pi}{2} \qquad [5.48]$$

$$\alpha=\pm\frac{(2k-1)}{2N}\pi \qquad [5.49]$$

Because we have imposed the ***cos(Nα) = 0*** condition, we know that ***sin(Nα) = 1*** and we are able to solve equation [5.46] as:

$$\sinh N\beta=\pm\frac{1}{\varepsilon} \qquad [5.50]$$

$$N\beta=\pm\sinh^{-1}\left(\frac{1}{\varepsilon}\right) \qquad [5.50]$$

$$\beta=\pm\frac{1}{N}\sinh^{-1}\left(\frac{1}{\varepsilon}\right) \qquad [5.51]$$

We return to equation [5.38], and equation [5.39] with the values of "a" identified in equation [5.49] above and b identified in equation [5.51] above and produce the LHP pole location equations as follows:

$$\sigma_p=-\frac{\sin\alpha\sinh\beta}{\varpi_0}=-\frac{\sin\left(\frac{(2k-1)}{2N}\pi\right)\sinh\left(\frac{1}{N}\sinh^{-1}\left(\frac{1}{\varepsilon}\right)\right)}{\varpi_0} \qquad [5.52]$$

$$\varpi_p=\frac{\cos\alpha\cosh\beta}{\varpi_0}=\frac{\cos\left(\frac{(2k-1)}{2N}\pi\right)\cosh\left(\frac{1}{N}\sinh^{-1}\left(\frac{1}{\varepsilon}\right)\right)}{\varpi_0} \qquad [5.53]$$

We are enabled to synthesize a Chebyshev filter as needed. We use equation [5.52] and equation [5.53] above because we have a closed form algebraic expression for the pole locations for all values of the possible parameters.

We can also manipulate the two equations into a slightly different form, as follows:

$$-\sin\alpha = \varpi_0 \frac{\sigma_p}{\sinh\beta} \qquad [5.54]$$

$$\cos\alpha = \varpi_0 \frac{\varpi_p}{\cosh\beta} \qquad [5.55]$$

Using the following identity, we have:

$$\sin^2\alpha + \cos^2\alpha = 1 = \omega_0^2\left[\left(\frac{\sigma_p}{\sinh\beta}\right)^2 + \left(\frac{\varpi_p}{\cosh\beta}\right)^2\right] \qquad [5.56]$$

$$\omega_0^2\left[\left(\frac{\sigma_p}{\sinh\left(\frac{1}{N}\sinh^{-1}\left(\frac{1}{\varepsilon}\right)\right)}\right)^2 + \left(\frac{\varpi_p}{\cosh\left(\frac{1}{N}\sinh^{-1}\left(\frac{1}{\varepsilon}\right)\right)}\right)^2\right] = 1 \qquad [5.57]$$

Equation [5.57] expresses the locus of an ellipse in the s-plane with a semi-minor axis given by equation [5.58] below, and a semi-major axis given by equation [5.59] below:

$$a = \omega_0 \sinh\left(\frac{1}{N}\sinh^{-1}\left(\frac{1}{\varepsilon}\right)\right) \qquad [5.58]$$

$$b = \omega_0 \cosh\left(\frac{1}{N}\sinh^{-1}\left(\frac{1}{\varepsilon}\right)\right) \qquad [5.59]$$

Algebraic manipulation allows equation [5.58] and equation [5.59] above to be redefined as follows

$$a = \frac{\omega_0}{2}\left\{\left(\frac{1}{\varepsilon} + \sqrt{1+\left(\frac{1}{\varepsilon}\right)^2}\right)^{1/N} - \left(\frac{1}{\varepsilon} + \sqrt{1+\left(\frac{1}{\varepsilon}\right)^2}\right)^{-1/N}\right\} \qquad [5.60]$$

$$b = \frac{\omega_0}{2}\left\{\left(\frac{1}{\varepsilon} + \sqrt{1+\left(\frac{1}{\varepsilon}\right)^2}\right)^{1/N} + \left(\frac{1}{\varepsilon} + \sqrt{1+\left(\frac{1}{\varepsilon}\right)^2}\right)^{-1/N}\right\} \qquad [5.61]$$

The definitions above permit the construction in the ***s***-plane of the Chebyshev filter from two Butterworth circles with radii equal to the semi-axes given and shown in figure 5.4 below.

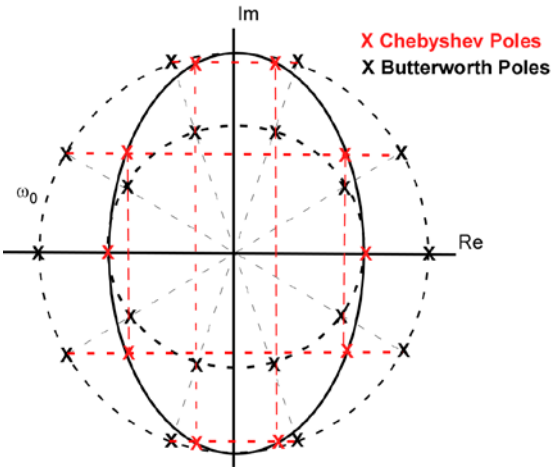

5.4 Pole Locations for 5th Order Chebyshev Filter

We note that the poles on the ellipse are entirely within the ω_0 circle. We find the un-normalized pole position as ω_{eff} as follows:

$$\varpi_{eff} = \varpi_0 \sqrt{\sigma_p^2 + \omega_p^2} \qquad [5.62]$$

From the characteristics of a complex-conjugate pole-pair, we find the ***Q*** factor from the ratio of σ_p/ω_p as follows:

$$\tan(\theta) = \frac{\sigma_p}{\varpi_p} = \frac{1}{\sqrt{(4Q^2 - 1)}} \qquad [5.63]$$

$$(4Q^2 - 1) = \left(\frac{\varpi_p}{\sigma_p}\right)^2 \qquad [5.64]$$

$$Q = \frac{1}{2}\sqrt{\left(\frac{\varpi_p}{\sigma_p}\right)^2 + 1} \qquad [5.65]$$

Table 5.1 below summarizes the pole locations for the ***5th*** order Chebyshev filter with 1dB ripple.

Table 5.1 - 5th Order Chebyshev Poles

σ_p	-0.08946	-0.23421	-0.289493341
ω_p	0.990107	0.61192	6.37727E-17

$\omega_{effective}$	0.99414	0.655208	0.289493341
Q	5.556441	1.398792	0.5

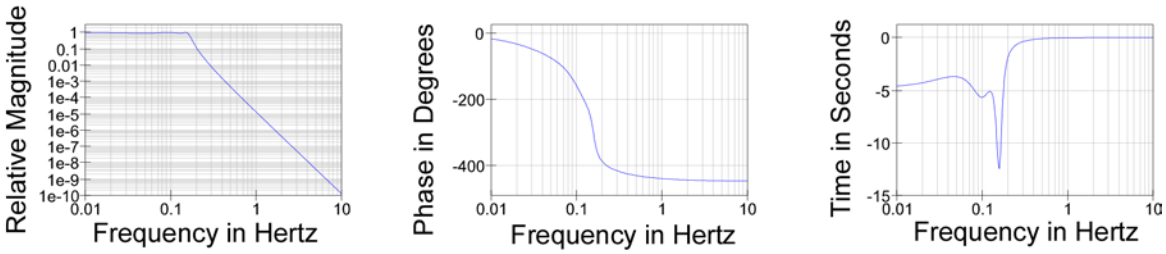

5.5 Magnitude, Phase, and Group Delay for 5th Order Chebyshev Filter

In figure 5.5 above, we show the magnitude, phase, and group delay responses for the 4th order Chebyshev filter, and in figure 5.6 below, we show its step response.

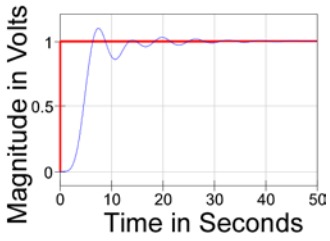

5.6 Step Response for 5th Order Chebyshev Filter

To enable comparison of the 5th order Chebyshev magnitude response with the 5th order Butterworth, we present the results in the same panel as shown in figure 5.7 below. We see that the Chebyshev filter with 1 dB of ripple below its characteristic frequency is nearly a decade better in attenuation above a common characteristic frequency in comparison to the Butterworth filter. The Chebyshev design is used where the ripple can be tolerated and improved selectivity near the characteristic frequency is needed.

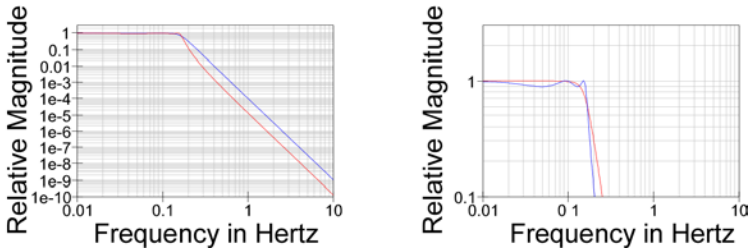

5.7 Magnitude Comparison for 5th Order Butterworth and Chebyshev Filter

To enable comparison of the 5th order Chebyshev step response with the 5th order Butterworth, we present the results in the same panel as shown in figure 5.8 below.

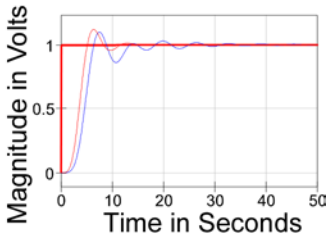

5.8 Step Response for 5th Order Butterworth and Chebyshev Filter

We see that greater group delay of the Chebyshev does not severely alter the overshoot, but the ringing of the higher Q factor poles makes its ringing much longer duration.

The inverse Chebyshev filter can be constructed following the same derivation path for the Chebyshev filter itself, but using the magnitude-squared definition in equation [5.66] below:

$$\left|H_{T_N}(j\Omega)\right|^2 = \frac{\varepsilon^2 T_N^2\left(1/\Omega\right)}{1+\varepsilon^2 T_N^2\left(1/\Omega\right)} = \frac{1}{1+\dfrac{1}{\varepsilon^2\left[\cos^2\left(N\cos^{-1}\left(1/\Omega\right)\right)\right]}} \qquad [5.66]$$

The Inverse Chebyshev filter is maximally flat in the pass-band, much like the Butterworth, but equal-ripple in its stop-band rejection. The notion of the inverse relationship extends to the pole and zero locations. The poles of equation [5.56] are derived as we have already done for the Chebyshev itself, but with the argument inverse. The poles of equation [5.56] are obtained by inverting the poles of the original Chebyshev filter in polar notation and each location. The poles are expressed as a magnitude and angle the inverse retains the angle but the magnitude is inverted. With the angle retained, the ***Q*** factor is invariant, but the ω_{eff} transforms to outside the enclosing semi-major axis circle.

The zeroes occur at frequencies determined by the numerator equation with the roots at:

$$N\cos^{-1}\left(1/\Omega\right) = \pm(2k-1)\frac{\pi}{2} \qquad [5.67]$$

$$\Omega = \sec\left[\frac{(2k-1)}{N}\frac{\pi}{2}\right] \qquad [5.68]$$

Table 5.2 - 5th Order Inverse Chebyshev Roots

$\omega_{effective}$	1.005894	1.526232	3.454310886
Q	5.556441	1.398792	0.5
ω_z	1.051462	1.701302	1.63246E+16

We plot the results for the Inverse-Chebyshev design based on the prior 5th order Chebyshev pole locations in figure 5.9 below.

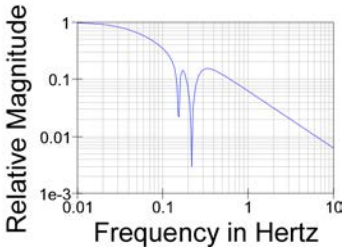

5.9 Magnitude Response for 5th Order Inverse Chebyshev Filter

The inverse Chebyshev filter is discussed here because it is the first design to introduce zeroes, but it is not used widely. The characteristic frequency defines the edge of the stop-band, rather than the pass-band. Also, the ripple factor for an inverse Chebyshev design must be pre-calculated from the desired stop-band characteristic and used in the predecessor prototype Chebyshev prior to inversion. The Inverse Chebyshev has a rejection in the stop-band bounded by the value given in equation [5.69] below.

$$Atten = \frac{1}{\sqrt{\left(\frac{1}{\varepsilon}\right)^2 + 1}} \qquad [5.69]$$

for attenuation of 60dB = .001, we solve for ε as follows:

$$\varepsilon = \frac{1}{\sqrt{\left(\frac{1}{Atten}\right)^2 - 1}} \qquad [5.70]$$

We see that ε is a small number and the prototype predecessor Chebyshev filter is much different from the example we have explored. Also, for N an odd order, the attenuation tends to a single pole roll-off, and to a constant for N an even order. There are much better filters

for selectivity than the Inverse Chebyshev, but they, too, are based on elliptic loci in the s-plane. The best selectivity of a pole-zero design can be obtained using a Cauer filter. Unfortunately, the derivation of the pole locations is even more involved than that for a Chebyshev design and will not be included here. Instead, we show that we can use a synthesized Cauer filter and show that we can approach much of its behavior as similar to the Chebyshev design.

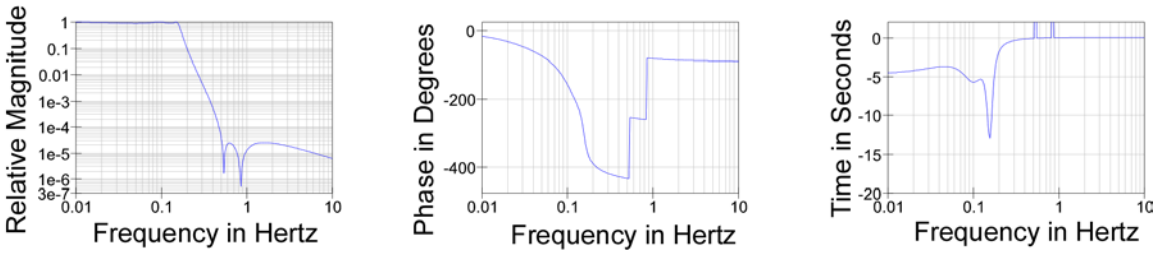

5.10 Magnitude, Phase, and Group Delay for 5th Order Cauer Filter

The Cauer design uses Elliptic functions to determine the pole positions in the pass-band, as well as in the stop-band. More parameters are required to determine the two dependent ripple behaviors. The 5th order design permits two zero pairs in the stop band, as well as the zero at infinity that produces the residual single-pole asymptote at the high end of the stop-band. The discontinuities in the phase response and group delay are artifacts of the plotting routine that is unable to interpret the rapid phase slopes through infinite-***Q*** zeroes. Phase response, as well as group delay in the stop-band should be interpreted as continuous.

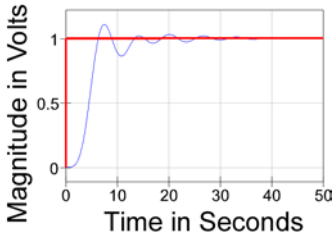

5.11 Step Response for 5th Order Cauer Filter

The step response for the 5th order Cauer filter design resembles that for the 5th order Chebyshev filter to which it is related. In figure 5.12 below, we show the magnitude response for each of the 5th order filters we have discussed (except the Inverse Chebyshev), alongside a detail panel.

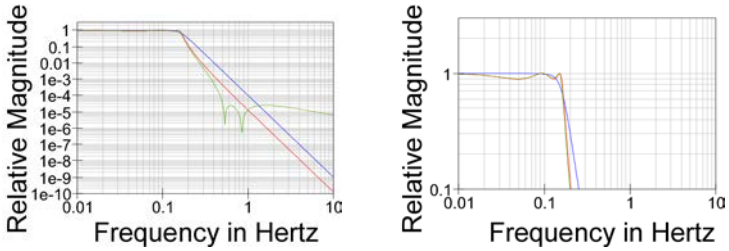

5.12 Magnitude Responses for 5th Order Butterworth, Chebyshev, and Cauer Filters

In figure 5.12 above, we see that the Butterworth filter has a monotonically decreasing magnitude function and tends to a 5-decade magnitude decrease per decade of frequency increase as expected in a 5th order design. In the detail, we see that the Butterworth filter is truly maximally flat prior to its characteristic frequency. The Chebyshev filter, also has a similar asymptotic rate, but near the characteristic frequency, it drops to a greater attenuation for every frequency above the same characteristic frequency as the Butterworth does. In the detail, it is also clear that the Chebyshev filter fluctuates between unity and a 0.9 magnitude, a value that translates to a 1 dB relative attenuation. We see in the detail in figure 5.12 above that the Cauer filter has a magnitude fluctuation over the same span and with nearly identical response, in comparison to the Chebyshev filter. In the first decade of frequency increase above the characteristic frequency, though, the Cauer filter has a magnitude that decreases at a faster rate than the Chebyshev filter, reaching the equal ripple level caused by the Cauer filter zero pattern before the Chebyshev filter. The Chebyshev filter continues with the constant 5-decade magnitude decrease per decade of frequency increase as expected in a 5th order design, but the Cauer filter provides its equal ripple level, ultimately returning to a single-pole 1-decade magnitude decrease per decade of frequency increase.

Despite the differences in performance at frequencies above the characteristic frequency, the 5th order Chebyshev filter and 5th order Cauer filter provide an excellent match in the pass-band and also the time domain responses as shown in the step response shown in figure 5.13 below.

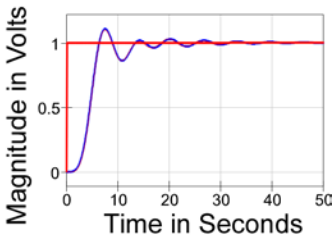

5.13 Step Response for 5th Order Chebyshev, and Cauer Filters

The excellent domain step responses shown in figure 5.13 above are related to the close match in group delay responses shown in figure 5.14 below.

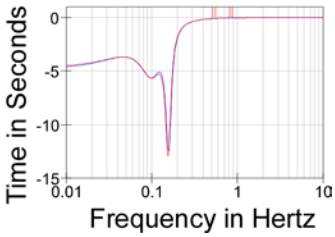

5.14 Group Delay for 5th Order Chebyshev, and Cauer Filters

We will use the closely matched group delay responses to use the Chebyshev filter behavior as a template for group delay equalization of the Cauer filter.

Each of the filter designs we have discussed thus far have increased the discrimination between the pass-band and the stop-band and improved selectivity. As each improvement was made, the group delay, overshoot and time-domain response got worse. If we approach the frequency separation issue between the pass-band and stop-band with the intent of keeping the group delay as constant as possible, we see there is another family of filter designs. We first introduced the ideal delay, represented as the multiplier e^{-sT} for any positive time index and showed the result in figure 2.4 for the one-second delay. We repeat that illustration here as figure 5.15 below for convenience..

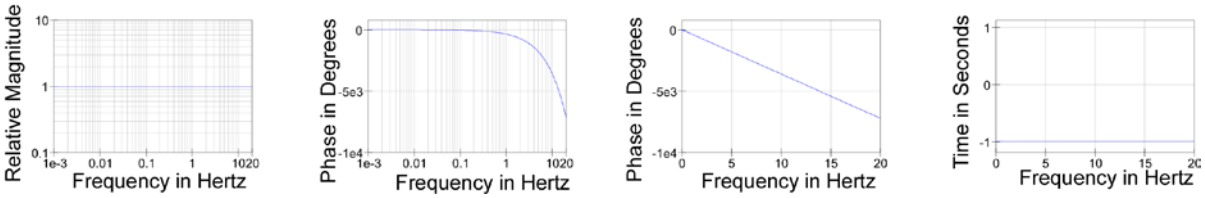

5.15 The Ideal One Second Delay Magnitude, Phase, and Group Delay Responses

If we start from the definition of the delay function, we can express a transfer function as:

$$H_{T_0}(s) = \frac{1}{e^{sT_0}} = \frac{1}{\cosh(sT_0) + \sinh(sT_0)} \qquad [5.71]$$

In equation [5.71] above, we have the entire transfer function, not the magnitude-squared function that we have employed in prior derivations. Thus, we can find the poles of equation [5.71] above by setting the denominator to zero and solving the resulting ***D(s)*** = 0 equation as follows.

$$\cosh(sT_0)+\sinh(sT_0)=0 \qquad [5.72]$$

We form a series expansion of the hyperbolic functions and perform a continued fraction expansion of the series at the degree we require.

$$\cosh(sT_0)=1+\frac{(sT_0)^2}{2!}+\frac{(sT_0)^4}{4!}+\frac{(sT_0)^6}{6!}+\frac{(sT_0)^8}{8!}+\frac{(sT_0)^{10}}{10!}+ \qquad [5.73]$$

$$\sinh(sT_0)=sT_0+\frac{(sT_0)^3}{3!}+\frac{(sT_0)^5}{5!}+\frac{(sT_0)^7}{7!}+\frac{(sT_0)^9}{9!}+\frac{(sT_0)^{11}}{11!}+ \qquad [5.74]$$

We illustrate by forming an approximation by expanding the denominator using a continued fraction expansion to the 5th order. To employ the method, we form the ratio with the greater degree polynomial in the denominator and perform long division. We begin the process with equation [5.75] below.

$$\frac{\cosh(sT_0)}{\sinh(sT_0)}=\frac{1}{sT_0}+\left\{\frac{1+\frac{(sT_0)^2}{2!}+\frac{(sT_0)^4}{4!}+\frac{(sT_0)^6}{6!}+}{sT_0\left(1+\frac{(sT_0)^2}{3!}+\frac{(sT_0)^4}{5!}+\frac{(sT_0)^6}{7!}+\right)}-\frac{1}{sT_0}\right\}$$

$$=\frac{1}{sT_0}+\left\{\frac{(1-1)+\left(\frac{(sT_0)^2}{2!}-\frac{(sT_0)^2}{3!}\right)+\left(\frac{(sT_0)^4}{4!}-\frac{(sT_0)^4}{5!}\right)+\left(\frac{(sT_0)^6}{6!}-\frac{(sT_0)^6}{7!}\right)+}{sT_0\left(1+\frac{(sT_0)^2}{3!}+\frac{(sT_0)^4}{5!}+\frac{(sT_0)^6}{7!}+\frac{(sT_0)^8}{9!}+\frac{(sT_0)^{10}}{11!}+\right)}\right\} \qquad [5.76]$$

$$\frac{\cosh(sT_0)}{\sinh(sT_0)}=\frac{1}{sT_0}+\left\{\frac{\frac{(3!-2!)}{3!\bullet 2!}(sT_0)+\frac{(5!-4!)}{5!\bullet 4!}(sT_0)^3+\frac{(7!-6!)}{7!\bullet 6!}(sT_0)^5+\frac{(9!-8!)}{9!\bullet 8!}(sT_0)^7+}{1+\frac{(sT_0)^2}{3!}+\frac{(sT_0)^4}{5!}+\frac{(sT_0)^6}{7!}+\frac{(sT_0)^8}{9!}+\frac{(sT_0)^{10}}{11!}+}\right\}$$

$$= \frac{1}{sT_0} + \left\{ \frac{\frac{1}{3}sT_0 + \frac{4}{5!}(sT_0)^3 + \frac{6}{7!}(sT_0)^5 + \frac{8}{9!}(sT_0)^7 + \frac{10}{11!}(sT_0)^9 + \frac{12}{13!}(sT_0)^{11} +}{1 + \frac{(sT_0)^2}{3!} + \frac{(sT_0)^4}{5!} + \frac{(sT_0)^6}{7!} + \frac{(sT_0)^8}{9!} + \frac{(sT_0)^{10}}{11!} +} \right\} \qquad [5.77]$$

After the series of transformations above, we are left with a remainder with the greater degree polynomial in the numerator, so we invert the fraction as follows, and iterate the same steps as above, adding terms from the original series as needed.

$$\frac{\cosh(sT_0)}{\sinh(sT_0)} = \frac{1}{sT_0} + \frac{1}{\left\{ \frac{1 + \frac{(sT_0)^2}{3!} + \frac{(sT_0)^4}{5!} + \frac{(sT_0)^6}{7!} + \frac{(sT_0)^8}{9!} + \frac{(sT_0)^{10}}{11!} +}{\frac{1}{3}sT_0 + \frac{4}{5!}(sT_0)^3 + \frac{6}{7!}(sT_0)^5 + \frac{8}{9!}(sT_0)^7 + \frac{10}{11!}(sT_0)^9 + \frac{12}{13!}(sT_0)^{11} +} \right\}}$$

$$= \frac{1}{sT_0} + \frac{1}{\frac{3}{sT_0} + \left\{ \frac{(sT_0)^2\left[\frac{1}{3!} - 3\frac{4}{5!}\right] + (sT_0)^4\left[\frac{1}{5!} - 3\frac{6}{7!}\right] + (sT_0)^6\left[\frac{1}{7!} - 3\frac{8}{9!}\right] + (sT_0)^8\left[\frac{1}{9!} - 3\frac{10}{11!}\right] +}{\frac{sT_0}{3}\left(1 + 3\frac{4}{5!}(sT_0)^2 + 3\frac{6}{7!}(sT_0)^4 + 3\frac{8}{9!}(sT_0)^6 + 3\frac{10}{11!}(sT_0)^8 + 3\frac{12}{13!}(sT_0)^{10} +\right)} \right\}}$$

$$= \frac{1}{sT_0} + \frac{1}{\frac{3}{sT_0} + \left\{ \frac{(sT_0)^2\left[\frac{8}{5!}\right] + (sT_0)^4\left[\frac{24}{7!}\right] + (sT_0)^6\left[\frac{48}{9!}\right] + (sT_0)^8\left[\frac{80}{11!}\right] + (sT_0)^{10}\left[\frac{120}{13!}\right]}{\frac{sT_0}{3}\left(1 + \frac{12}{5!}(sT_0)^2 + \frac{18}{7!}(sT_0)^4 + \frac{24}{9!}(sT_0)^6 + \frac{30}{11!}(sT_0)^8 + \frac{36}{13!}(sT_0)^{10} +\right)} \right\}}$$

$$= \frac{1}{sT_0} + \frac{1}{\frac{3}{sT_0} + \left\{ \frac{\frac{sT_0}{5} + (sT_0)^3\left[\frac{72}{7!}\right] + (sT_0)^5\left[\frac{144}{9!}\right] + (sT_0)^7\left[\frac{240}{11!}\right] + (sT_0)^9\left[\frac{360}{13!}\right]}{1 + \frac{12}{5!}(sT_0)^2 + \frac{18}{7!}(sT_0)^4 + \frac{24}{9!}(sT_0)^6 + \frac{30}{11!}(sT_0)^8 + \frac{36}{13!}(sT_0)^{10} +} \right\}} \qquad [5.78]$$

We continue the fraction expansion as:

$$\frac{\cosh(sT_0)}{\sinh(sT_0)} = \frac{1}{sT_0} + \cfrac{1}{\frac{3}{sT_0} + \cfrac{1}{\frac{5}{sT_0} + \cfrac{1}{\frac{7}{sT_0} + \cfrac{1}{\frac{9}{sT_0} + \cfrac{1}{\frac{11}{sT_0} + \bullet\bullet\bullet}}}}}} \qquad [5.79]$$

We choose a 5th order solution, so we truncate and solve:

$$\frac{\cosh(sT_0)}{\sinh(sT_0)} \cong \frac{1}{sT_0} + \cfrac{1}{\frac{3}{sT_0} + \cfrac{1}{\frac{5}{sT_0} + \cfrac{1}{\frac{7}{sT_0} + \frac{sT_0}{9}}}} = \frac{1}{sT_0} + \cfrac{1}{\frac{3}{sT_0} + \cfrac{1}{\frac{5}{sT_0} + \cfrac{1}{\frac{63}{9sT_0} + \frac{(sT_0)^2}{9sT_0}}}} \qquad [5.80]$$

$$\frac{\cosh(sT_0)}{\sinh(sT_0)} \cong \frac{1}{sT_0} + \cfrac{1}{\frac{3}{sT_0} + \cfrac{1}{\frac{5}{sT_0} + \frac{9sT_0}{(sT_0)^2 + 63}}} = \frac{1}{sT_0} + \cfrac{1}{\frac{3}{sT_0} + \cfrac{1}{\frac{5(sT_0)^2 + 315 + 9(sT_0)^2}{(sT_0)^3 + 63sT_0}}} \qquad [5.81]$$

$$\frac{\cosh(sT_0)}{\sinh(sT_0)} \cong \frac{1}{sT_0} + \cfrac{1}{\frac{3}{sT_0} + \cfrac{1}{\frac{5}{sT_0} + \frac{9sT_0}{(sT_0)^2 + 63}}} = \frac{1}{sT_0} + \cfrac{1}{\frac{3}{sT_0} + \cfrac{1}{\frac{5(sT_0)^2 + 315 + 9(sT_0)^2}{(sT_0)^3 + 63sT_0}}} \qquad [5.82]$$

$$\frac{\cosh(sT_0)}{\sinh(sT_0)} \cong \frac{1}{sT_0} + \cfrac{1}{\frac{3}{sT_0} + \frac{(sT_0)^3 + 63(sT_0)}{14(sT_0)^2 + 315}} \qquad [5.83]$$

$$\frac{\cosh(sT_0)}{\sinh(sT_0)} \cong \frac{1}{sT_0} + \cfrac{1}{\frac{3\left(14(sT_0)^2 + 315\right) + (sT_0)^4 + 63(sT_0)^2}{sT_0\left(14(sT_0)^2 + 315\right)}} \qquad [5.84]$$

$$\frac{\cosh(sT_0)}{\sinh(sT_0)} \cong \frac{1}{sT_0} + \frac{14(sT_0)^3 + 315(sT_0)}{(sT_0)^4 + 105(sT_0)^2 + 945} \quad [5.85]$$

$$\frac{\cosh(sT_0)}{\sinh(sT_0)} \cong \frac{15(sT_0)^4 + 420(sT_0)^2 + 945}{(sT_0)^5 + 105(sT_0)^3 + 945(sT_0)} \quad [5.86]$$

Therefore, we sum the cosh(***sT₀***) and sinh(***sT₀***) polynomials to obtain the poles:

$$(sT_0)^5 + 15(sT_0)^4 + 105(sT_0)^3 + 420(sT_0)^2 + 945(sT_0) + 945 = 0 \quad [5.87]$$

$$\frac{1}{945}(sT_0)^5 + \frac{15}{945}(sT_0)^4 + \frac{105}{945}(sT_0)^3 + \frac{420}{945}(sT_0)^2 + (sT_0) + 1 = 0 \quad [5.88]$$

$$H_{T_0}(s) = \frac{945}{(sT_0)^5 + 15(sT_0)^4 + 105(sT_0)^3 + 420(sT_0)^2 + 945(sT_0) + 945} \quad [5.89]$$

The transfer function in equation [5.89] above defines a 5th order Bessel filter. We find the roots numerically and present the results in table 5.3 below.

Table 5.3 - 5th Order Bessel Roots

σ_p	**2.324674**	**3.351956399**	**3.646738595**
ω_p	**3.571023**	**1.742661416**	
$\omega_{effective}$	**4.261023**	**3.777893661**	**3.646738595**
Q	**0.916477**	**0.563535621**	**0.5**

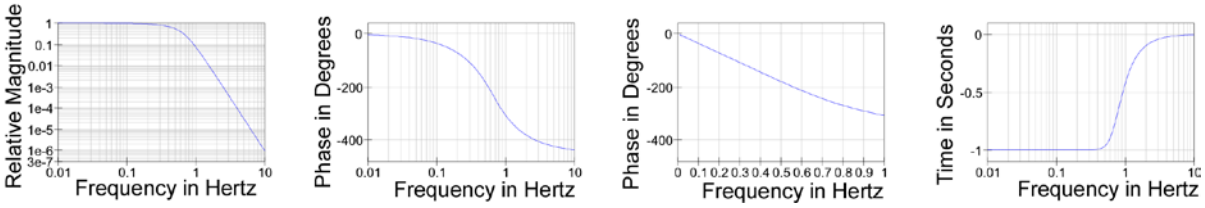

5.16 Magnitude, Phase (Log and Lin), and Group Delay for 5th Order Bessel Filter

We see in figure 5.16 above that the Bessel filter has a monotonic decrease in magnitude as the frequency increases and asymptotic 5th order decrease associated with a five-pole behavior. For frequencies below its characteristic frequency at ~0.7Hz for the 1-second

delay, the magnitude is not as flat as the 5th order Butterworth, and certainly not as selective as the Chebyshev or Cauer filters. The Bessel filter, however, does exhibit the flat group delay characteristic that the design objective set. The flat group delay is shown in the far right panel and the relationship to the linear phase is seen in the panel adjacent to the group delay. The result of the flat delay characteristic is to obtain the step response shown in figure 5.17 below.

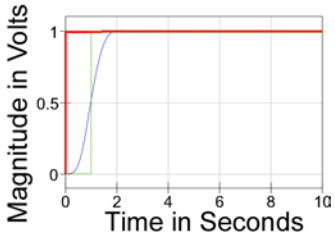

5.17 Step Response for 5th Order Bessel Filter with Ideal for Reference

We see in figure 5.17 above that the response curve passes the 50% magnitude very near the 1-second delay as promised by the design objective. The response is obtained with nearly no over-shoot as expected from all frequency components experiencing the same delay. The Bessel filter may offer sufficient selectivity for some applications, but for those applications requiring both good frequency domain selectivity and time domain response, the solution may require adding a delay equalizer to a filter with the requisite selectivity.

6.0 Delay Equalizers

Delay equalizers are constructed from the class of All-Pass filters. All pass filters are constructed with a frequency-dependent phase behavior, but a unity-magnitude transfer function. To achieve the behavior, the all pass filter employs poles in the LHP and zeroes in the RHP at mirror image locations as shown in figure 6.0 below.

In figure 6.0 below we show the pole-zero plot in the s-plane with the poles taken from the Butterworth 4th and 5th order filter example. We have added RHP zeros in mirror image locations and shown the phasors for the highest frequency Pole-Zero (PZ) pair for discussion in each panel.

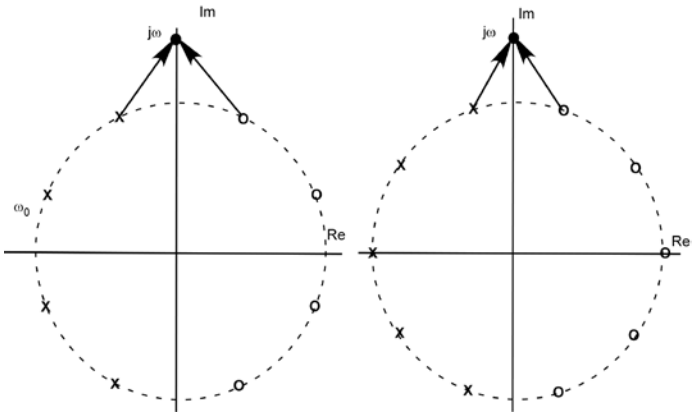

6.0 All Pass Filter 4th Order and 5th Order Pole Locations with Phasors for 2 PZ Pairs

Because the poles are the roots of the denominator ***D(s)*** polynomial and the zeroes are the roots of the numerator ***N(s)*** polynomial, we can construct phasor pairs for each PZ pair in the all pass filter. Each phasor must have the same magnitude or length from the mirror image location to the $j\omega$ excitation locus on the imaginary axis. Therefore, the magnitude ratio for mirror image PZ pairs is unity for all pairs. We see also that the phasor angles are complement to each other. We equate $\theta_p = -\theta_z$ for the phasor pairs, but note that the contribution from the numerator of a transfer function adds angles and from the denominator of subtracts angles. The result is a transfer function with unity magnitude and twice the phase contribution from the LHP poles alone.

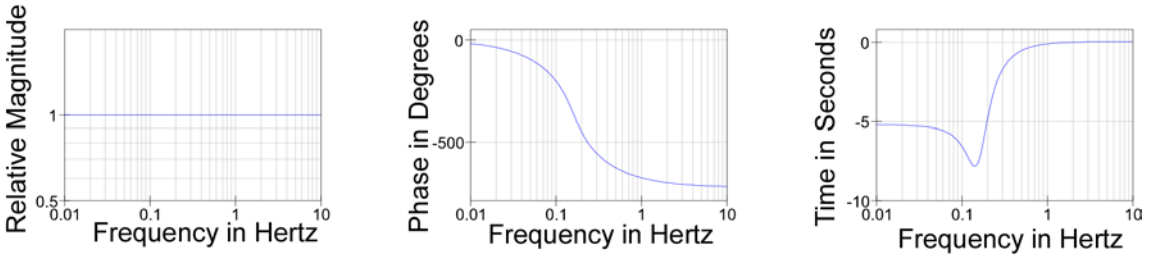

6.1 All Pass Filter 4th Order Magnitude, Phase, and Group Delay

We see in figure 6.1 above that the magnitude is indeed unity across the entire frequency span for the 4th order all pass filter. We see also that the center panel of figure 6.1 above indicates twice the phase angles as the 4th order Butterworth filter with the same pole locations as indicated in figure 5.1 in the previous section. Likewise, the consequent group delay is twice that of the 4th order Butterworth filter also as shown in the similar rightmost panels of the figures for each implementation.

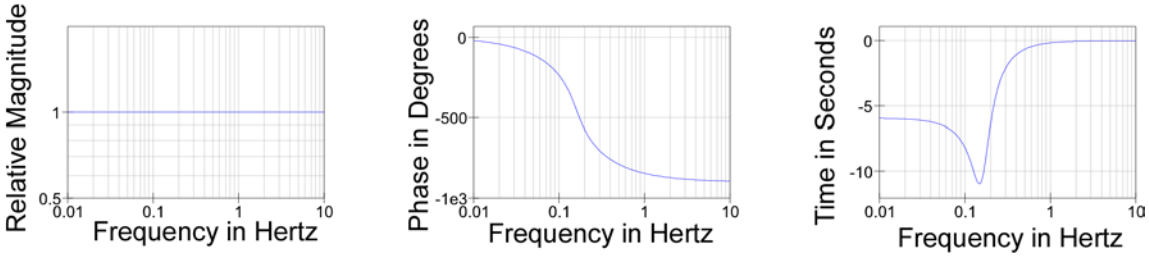

6.2 All Pass Filter 5th Order Magnitude, Phase, and Group Delay

We see in figure 6.2 above that the magnitude is also unity across the entire frequency span for the 5th order all pass filter, too. We see also that the center panel of figure 6.2 above indicates twice the phase angles as the 5th order Butterworth filter with the same pole locations as indicated in figure 5.2 in the previous section. Likewise, the consequent group delay is twice that of the 5th order Butterworth filter also as shown in the similar rightmost panels of the figures for each implementation.

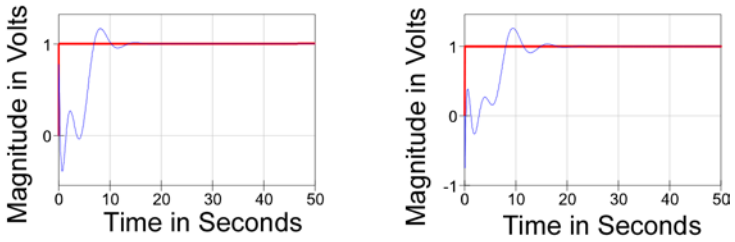

6.3 All Pass Filter 4th and 5th Order Step Response

The step responses of the 4th and 5th order all pass filters are shown for completeness in figure 6.3 above. For these realizations there is no apparent use for this behavior.

We use a goal-seeking algorithm to produce an equal ripple approximation to a flat delay characteristic for the 5th order Chebyshev and Cauer filter designs we have explored in the previous section.

The goal seeking algorithm produced the set of 5th order equalizer poles shown in table 6.0 below, along with an additional pole pair for a 7th order equalizer. The goal for the 5th order equalizer was set to produce an equal ripple delay up to and including the delay for the 5th order Chebyshev and Cauer filters. The goal for the additional pole pair was to include its delay at a frequency higher than the combined prior effects.

Table 6.0 - 5th & 7th Order Equalizer

Pole #	1	2	3	4
$\omega_{effective}$	0.833	0.320	0.752	1.25
Q	0.5	0.68	1.8	5

We show the results for the 5th order sections\ group delay contributions in figure 6.4 below.

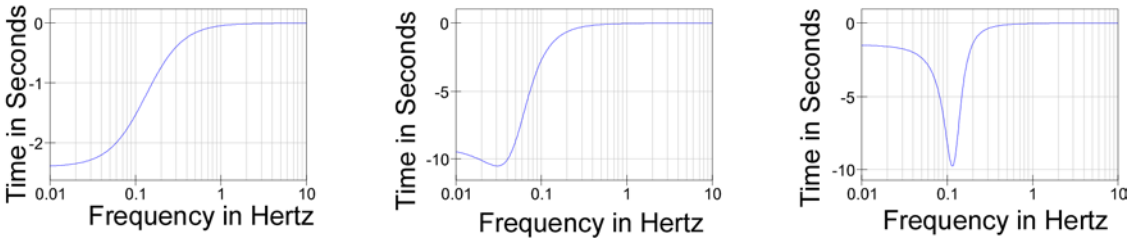

6.4 All Pass Filter Section Group Delay Plot for Table 6.0 – Pole 1, Pole 2, and Pole 3

We combine a cascade of the sections found in figure 6.4 above to produce the 5th order equalizer shown in figure 6.5 below.

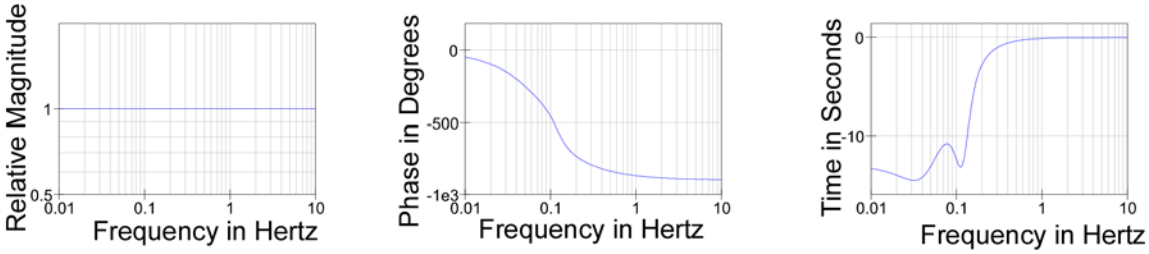

6.5 All Pass 5th Order Equalizer Magnitude, Phase, and Group Delay

The 5th order equalizer group delay we found does not have an intuitive delay dependency in figure 6.5 above, until we add the delay to the group delay for the 5th order Chebyshev or Cauer filter to produce the magnitude and group delay results in figure 6.6 below.

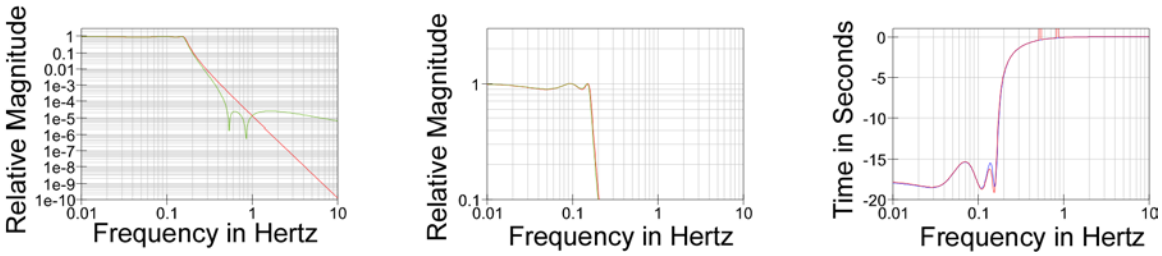

6.6 All Pass 5th Order Equalizer Applied to Chebyshev, and Cauer Filters

The 5th order equalizer group delay we found complements the filter delay to make the sum nearly constant, as shown in figure 6.6 above, and in detail in figure 6.7 below.

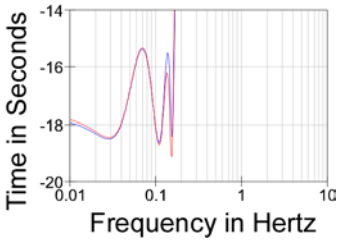

6.7 All Pass 5th Order Equalized Detail for Chebyshev, and Cauer Filters

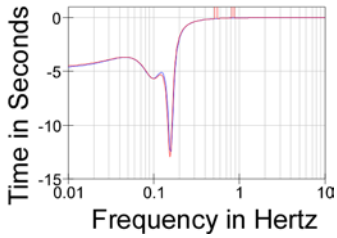

6.8 Group Delay for 5th Order Chebyshev, and Cauer Filters without the Equalizer

We see in figure 6.8 above that both the Chebyshev and Cauer filters exhibit a group delay variation that spans from about 4 seconds to about 13 seconds, or a 9 second difference. The 5th order equalizer has increased the total group delay by adding delay at low frequencies in a pattern that makes the sum more nearly constant. The variation is reduced to near a 2 second delay difference in the pass band, or a reduction to about 4 times smaller variation. Higher order equalizers can achieve flatter results with less variation than the 5th order example above. With the equalizer, and without it, we show the step response behaviors in figure 6.9 below.

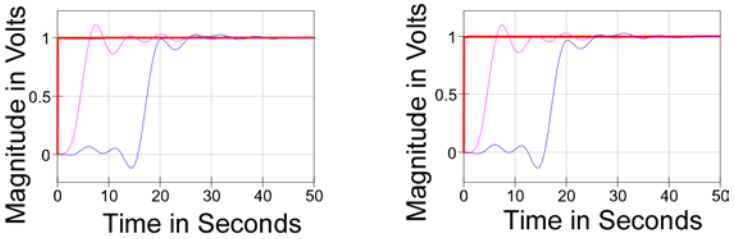

6.9 Step Responses for 5th Order Chebyshev, and Cauer Filters

We see in figure 6.9 above that both the Chebyshev and Cauer filters exhibit less overshoot and reduced ringing after the transition than the results without equalization. The Chebyshev result is on the left and the Cauer is on the right, but the difference is nearly indistinguishable. The 5th order equalization utilizes the group delay of the highest frequency pole of the filter, adding delay at lower frequencies to flatten the composite delay. Because the highest frequency pole of the original filter has its highest Q factor also, it contributes the peak delay to the summation. Unfortunately, the filter bandwidth extends to higher frequencies than that peak group delay and the lower group delay at higher frequencies allows high frequency components to arrive with less delay than lower frequency components. The lack of group delay above the highest frequency pole is the cause of the under-shoot and ringing before the equalized transition occurs. We have added another ple pair all pass section, making the equalizer a 7th order solution. That pole is listed as pole number 4 in table 6.0 and occurs at a higher frequency than the peak group delay of the original 5th order filters. In figure 6.10 below we show the group delay contribution for this new pole pair.

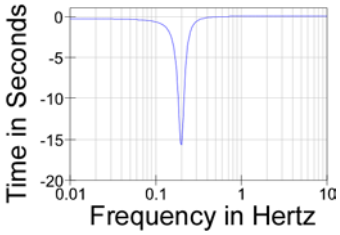

6.10 All Pass Section Group Delay for 7th Order Equalizer Augmentation

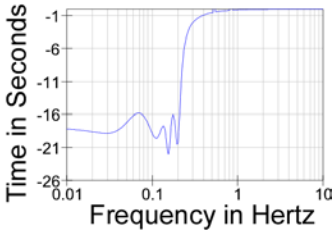

6.11 Group Delay of All Pass 7th Order Equalizer Applied to Cauer Filter

We see in figure 6.11 above that the additional group delay adds another peak to the response at a higher frequency and above the highest prior peak delay frequency. The effect of the additional delay bandwidth is a slight improvement in both the undershoot and ringing as shown in figure 6.12 below.

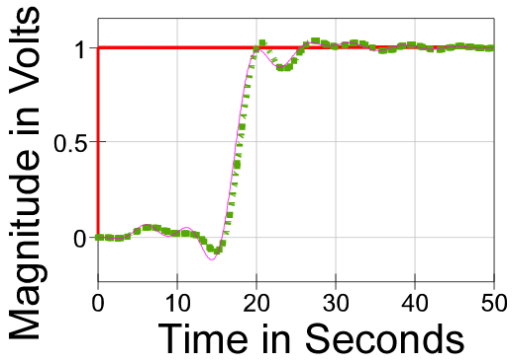

6.12 Step Response for 5th Order Cauer Filter with 5th and 7th Order Equalizers

We see in figure 6.12 above in the plot in green dots that the extra equalization improves the under-shoot prior to the response transition, but more equalization is apparently required to flatten the response even more.

7.0 Frequency Domain Transformations

In prior sections we have explored low-pass filter designs. We have not included high-pass and band pass examples because there are effective transformations to convert a low-pass filter to high-pass and band-pass designs. To transform a prototype low-pass design to a high-pass function, each occurrence of the ***s***-plane operator in the low-pass transfer function is replaced by the substitution of ***(ω0/s)*** in the equation. For example, the single pole low-pass is transformed in equation 7.0 below.

$$H_{LP}(s)=\frac{1}{(s+1)} \Rightarrow H_{HP}(s)=\frac{1}{\left(\omega_0/s+1\right)}=\frac{s}{(s+\omega_0)}=\frac{s/\omega_0}{\left(s/\omega_0+1\right)} \qquad [7.0]$$

To transform a prototype low-pass design to a band-pass function, each occurrence of the ***s***-plane operator has its occurrence replaced by the substitution of:

$$s \Rightarrow \frac{\omega_0}{\omega_U-\omega_L}\left(\frac{s}{\omega_0}+\frac{\omega_0}{s}\right)=\frac{s^2+\omega_0^2}{s(\omega_U-\omega_L)} \qquad [7.1]$$

For example, the single pole low-pass is transformed in equation 7.2 below.

$$H_{LP}(s)=\frac{1}{(s+1)}\Rightarrow H_{BP}(s)=\frac{1}{\left(\frac{s^2+\varpi_0^2}{s(\varpi_U-\varpi_L)}+1\right)}=\frac{s(\varpi_U-\varpi_L)}{s^2+s(\varpi_U-\varpi_L)+\varpi_0^2} \qquad [7.2]$$

Other circuit-level transformations are possible for low-pass to band-pass using a Weaver modulator, but that is beyond the scope of this course.

8.0 Summary and Conclusions

This course has defined the notation for roots of polynomial expressions describing Linear-Time Invariant (LTI) systems in the frequency domain, and related the operator notation to the time-domain response using complex exponential notation. A single pole circuit was introduced and responses analyzed in the frequency domain and time domain. An ideal delay was introduced for comparison and to set a reference for step response behaviors.

Polynomial root locations were described in the complex ***s***-plane and complex conjugate pairs plotted and described using ***(ω_0, ζ)*** notation as well as ***(τ_0, Q)*** notation. Phasor notation was introduced for evaluation of steady-state sinusoidal excitation of transfer functions. Second-order, complex conjugate pole pairs were introduced and the asymptotic behaviors developed and contrasted to the single-pole behaviors in magnitude, phase, and group delay attributes. Straight-line approximations were produced and the errors of approximation discussed.

Classical Butterworth, Chebyshev, and Bessel filters were introduced and the construction formulae developed. The Cauer filter was also illustrated, but mathematical development not included. Frequency domain and time domain responses were developed using a 4^{th} order form as representative of even-order forms and a 5^{th} order design as representative of odd-order forms. Only the 5^{th} order Bessel filter example was synthesized from the equations. A 5^{th} order equalizer was developed for the 5^{th} order Chebyshev and Cauer filter and shown to provide equivalent results. An additional pole pair was added to the 5^{th} order equalizer and the justification and improvements noted. Transformations were discussed to convert low-pass prototype designs to high-pass and band-pass filters.

